Audio Engineering Society

Convention Paper 10082

Presented at the 145th Convention
2018 October 17 – 20, New York, NY, USA

Microphone Array Geometry for Two Dimensional Broadband Sound Field Recording

Wei-Hsiang Liao, Yuki Mitsufuji, Keiichi Osako, and Kazunobu Ohkuri

Sony Corporation, Audio Technology Development Department, Tokyo, Japan

Correspondence should be addressed to Kazunobu Ohkuri (Kazunobu.Ohkuri@sony.com)

ABSTRACT

Sound field recording with arrays made of omnidirectional microphones suffers from an ill-conditioned problem due to the zero and small values of the spherical Bessel function. This article proposes a geometric design of a microphone array for broadband two dimensional(2D) sound field recording and reproduction. The design is parametric with a layout having a discrete rotationally symmetric geometry composed of several geometrically similar subarrays. The actual parameters of the proposed layout can be determined for various acoustic situations to give optimized results. This design has the advantage that it simultaneously satisfies many important requirements of microphone arrays such as error robustness, operating bandwidth, and microphone unit efficiency.

1 Introduction

The importance of sound field recording in the audio industry has been increasing recently. Using wave field synthesis techniques [1], an auditory scene within a space can be reproduced and manipulated to deliver highly realistic perceptual experiences. A sound field is usually recorded by recording sound pressure values with omnidirectional microphones at several sampling positions within a volume of space. If appropriate sampling positions are selected, then it is sufficient to reconstruct sound pressure values throughout the whole volume using only the sounds recorded at sampling positions [2] [3]. The reconstruction procedure is briefly summarized as follows: first project the recorded sound pressures onto a suitable mode domain (e.g., spherical or cylindrical harmonic domain) to form a vector of harmonic coefficients, then use it to derive pressure values of non-sampling positions within the volume.

In such applications, sounds may originate from any direction. Therefore, isotropic geometries are usually favored over linear ones, such as circular and spherical designs [4]. In these designs, microphones are arranged in a uniform or nearly uniform manner on a circle or a sphere. However, when these designs are used to record an actual sound field, the mode domain projection become erroneous at some frequencies. This is because, in some frequency bands, these designs are prone to error due to the zero points in their mode functions. The mode functions are Bessel functions for circular arrangements and spherical Bessel functions for the spherical arrangements. The zeros of mode functions for circular arrangements are depicted in Fig. 1(a). This problem is also known as the *Bessel zero problem* or the *forbidden frequency problem* [4] [5]. There are several ways of dealing with the Bessel zero problem, which require either redundant microphone units [6] (Fig. 1(b)), cardioid microphones (Fig. 1(c)) [7], or a rigid baffle [8]. In many situations, these approaches are not feasible due to cost or physical limitations. On

the other hand, the Bessel zero problem is only a special case of a much more general problem. Such generalization has been considered by Rafaely [9]. In his work, he considered the problem caused by Bessel zeros as a consequence of an ill-conditioned inverse problem. The ill-conditioning makes the sound field reconstruction process extremely sensitive to errors and noises. Measurement noise is usually unavoidable (e.g., inherent sensor noise, environmental noise). Moreover, it is difficult to perfectly set up the physical array; the coordinates of microphone units may drift from the theoretical positions, due to imperfect placement or limited manufacturing accuracy. These errors will be magnified by the reciprocal of small values of the mode function in the reconstruction/reproduction procedure, causing a serious numerical problem. Therefore, during the design stage, instead of simply avoiding the zeros in Bessel functions, it is preferable to consider the problem in the form of maximizing error robustness. Therefore, the design process of a sound field recording array can be considered as an optimization problem. The goal of the optimization is to distribute microphone units in the space in which the resulting sampling geometry has the best or approximately best error robustness. Relevant constraints such as the size of the microphones, the maximum acceptable condition number within the frequency of interest, and the isotropy of the array should also be considered. Furthermore, appropriate regularization is required. In this article, we use spatial resolution control to achieve the regularization.

The proposed design constructs a sound field recording array by combining multiple concentric circular arrays, in which microphone units are distributed in an equiangular manner with respect to the global origin. Comparing the proposed array designs with the conventional circular array, better overall condition can be achieved with ordinary pressure microphones and heuristic parameters. Further improvements can be obtained by using optimized parameters.

This article is organized as follows. The introduction describes the Bessel zero problem in sound field reconstruction. The following section explains the fundamental signal processing steps with circular or spherical harmonics. In the next three sections, the first proposes a parametric set of properties for constructing error-robust geometries. The second addresses how to apply spatial resolution control to the transformation matrices of proposed geometries. The third section explains the optimization process including the constraints proposed in the previous sections and shows some exemplar optimized parameters. The subsequent analysis section compares the proposed design with conventional designs and the last section concludes the article.

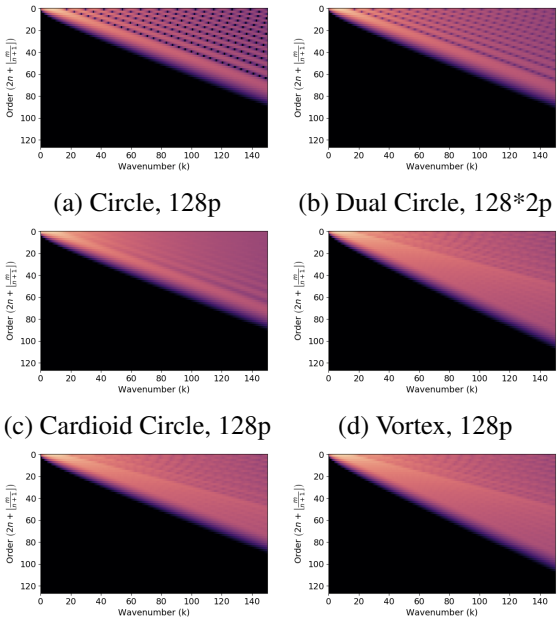

(a) Circle, 128p (b) Dual Circle, 128*2p

(c) Cardioid Circle, 128p (d) Vortex, 128p

(e) Floral, 128p (f) Random, 128p

Fig. 1: Maximum value of mode functions for different arrays, $\max_q b_n(kr_q)$, for various array designs. Black areas indicate minuscule values below 60dB. The wavenumber range in the figure corresponds to the frequency range of $0-8$kHz.

2 Signal Processing in Spherical Harmonics Domain

Conventional sound field recording and reconstruction can be achieved by obtaining the cylindrical or spherical harmonic coefficients of the sound field. In the case of a circular array, if the condition of the Shannon–Nyquist sampling theorem holds [10], the coefficients a_{mn} can be found by sampling the pressure of the sound field p with Q sampling points, then removing the radial dependent mode function, $b_n(kr)$, with a_{mn} divided as follows [9]:

$$a_{mn}(k) = \sum_{q=0}^{Q-1} \frac{p_k(r,\theta_q,\phi_q)}{b_n(kr)} Y_n^{m*}(\theta_q,\phi_q),\ |m| \le n. \quad (1)$$

In (1), k is the wavenumber, where $k = 2\pi f/c_s$, c_s is the sound speed, and f is the frequency. In the case of an open spherical array with omnidirectional microphones, $b_n(kr)$ is the spherical Bessel function, r is the radius, and $Y_n^{m*}(\theta_q,\phi_q)$ is the spherical harmonic of degree m and order n [5]. Alternatively, if a height-invariant sound field is assumed and the array is circular, then the spherical harmonics are replaced by cylindrical harmonics $C_m(\phi_q)$ as follows:

$$a_{mn}(k) = \sum_{q=0}^{Q-1} \frac{p_k(r,\phi_q)}{b_n(kr)} C_m(\phi_q),\ |m| = n. \quad (2)$$

The step of dividing $b_n(kr)$ in (1) and (2) is sometimes referred to as *mode compensation* [11]. The division causes a numerical problem if $b_n(kr)$ is nearly zero (Bessel zero problem). The process of estimating $a_{mn}(k)$ can be extended to deal with noncircular or nonspherical arrays. Again, if the condition of the Shannon–Nyquist sampling theorem holds, even if the elements of an array do not have a common radius, the sampled pressure field can be expressed as

$$p_k(r_q,\theta_q,\phi_q) = \sum_{n=0}^{N} \sum_{m=-n}^{n} a_{mn}(k) b_n(kr_q) Y_n^{m*}(\theta_q,\phi_q). \quad (3)$$

In this case, the estimated spherical harmonic coefficients a_{mn} can be obtained by applying a transform matrix to the sampled pressure field p as follows:

$$a_{mn}(k) = \mathbf{B}_k^{\dagger} p_k,$$

$$p_k = \begin{bmatrix} p_k(r_0,\theta_0,\phi_0), \\ p_k(r_1,\theta_1,\phi_1), \\ \vdots \\ p_k(r_L,\theta_L,\phi_L) \end{bmatrix},\ L = Q-1, \quad (4)$$

$$\mathbf{B}_k = \begin{bmatrix} b_0(kr_0)Y_0^0(\theta_0,\phi_0) & \cdots & b_N(kr_0)Y_N^N(\theta_0,\phi_0) \\ \vdots & \ddots & \vdots \\ b_0(kr_L)Y_0^0(\theta_L,\phi_L) & \cdots & b_N(kr_L)Y_N^N(\theta_L,\phi_L) \end{bmatrix}. \quad (5)$$

In (4), p_k is the measured vector of the sampled pressure field p at wavenumber k. The division in the mode compensation step is replaced by a pseudoinverse $B_k^{\dagger}$ in (4). To obtain an accurate result, the transform matrix B_k must be invertible and well-conditioned. The condition of B_k can be measured by its condition number $\kappa(B_k)$, where

$$\kappa(k) = \|B_k\| \cdot \|B_k^{\dagger}\| = \frac{\overline{\sigma}(B_k)}{\underline{\sigma}(B_k)}. \quad (6)$$

In (6), $\|\cdot\|$ denotes the l^2-norm, and $\underline{\sigma}, \overline{\sigma}$ are the smallest and the largest singular values of B_k, respectively. The condition number κ indicates that if there is an error or perturbation in the measured vector, the error will be amplified by a factor of κ [12]. A smaller condition number indicates better condition and, thus, stronger error robustness. If κ is very large, then the matrix is considered as ill-conditioned. The error-robustness analysis of circular and spherical arrays based on the condition number was reported in detail in [4]. To obtain a well-conditioned B_k, the geometry of the sampling points must enable the sampling of a sufficient number of independent modes within the volume of space, while the sampling weights for the modes should be within an order of magnitude. This agrees with the 'inconsistent' requirement of compressed sensing [2].

A conceptual workflow of sound field recording and reconstruction is presented in Fig. 2. The multichannel signal recorded by the array is first transformed by an STFT (short-time Fourier transform) then an SHT (spherical harmonic transform), as in (1). The SHT can be replaced by a cylindrical transform if a 2D case is assumed, as in (2). Then transform matrices are generated from the array geometry information and a spatial resolution control is applied to each STFT bin. The mode compensation block multiplies the pseudoinverse of transformation matrix to the recorded signal and outputs the harmonic coefficients, a_{mn}. The harmonic coefficients obtained from the recording can be used to generate drive signals according to the actual speaker array configuration. The drive signal can be generated by applying the inverse of the speaker response or other existing algorithms [1] [13] [14].

3 Geometry Design

As described in previous sections, the design of the geometry is a constrained optimization problem. The

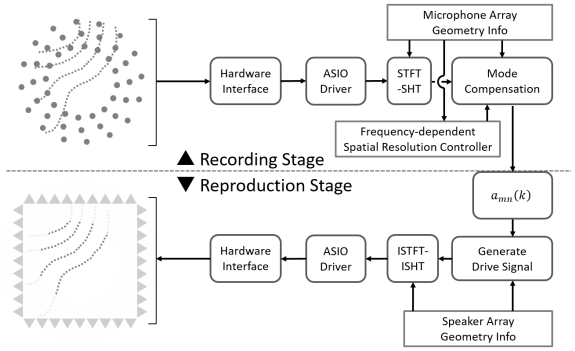

Fig. 2: Block diagram of the signal processing workflow.

optimization process searches for a distribution of microphone units within a volume of space such that the resulting transform matrices are well-conditioned and all constraints are satisfied. Unfortunately, such an optimization problem is in general a nonsmooth quasi-convex problem [15], for which it is difficult to apply conventional gradient-based optimization algorithms. Moreover, the solution space is so large that utilizing metaheuristic algorithms also becomes impractical.

The solution space can be reduced by restricting how the array is constructed. Since the sound field recording array is preferably isotropic and the signal processing operates in the spherical/cylindrical harmonics domain, it is reasonable to construct the array as several concentric isotropic subarrays with the microphone units of the whole array distributed in an equiangular manner. With this construction, the number of parameters can be greatly reduced such that the new solution space is sufficiently small, therefore the use of metaheuristic algorithms becomes feasible. The extra constraints mentioned in the previous section are applied during the optimization process. Such constraints include the minimal distance between microphone units due to physical limits and the maximum tolerance of worst-case condition within the frequency range of interest. Utilizing the optimized sampling geometry with suitable regularization, sound fields can be recorded and reconstructed with satisfactory accuracy.

To summarize, the proposed set of geometric designs possess the following properties:

Geometrically similar subarrays The array is composed of several geometrically similar subarrays, each consisting of multiple microphone units. Any two subarrays can be made to coincide by scaling, rotation, and reflection. Arrays created in this manner have discrete rotational symmetry.

Equiangular distribution All the microphone units become uniformly distributed when projected onto a circle centered at the origin. This arrangement helps reduce the complexity of signal processing and provides downward scalability.

Arithmetically progressive radii The radii of the subarrays form a generalized arithmetic sequence. According to our experimental results, radii in an arithmetic progression achieve slightly better matrix condition than those in logarithmic or geometric sequences, which appeared in previous works [16] [17]. In the experiment, we assume that 128 microphones are used, then we find the optimal common difference and the optimal common ratio for arithmetic and geometric progressions, respectively. However, further investigation is required to establish whether the optimality of arithmetic progression is a general phenomenon.

Some examples of proposed designs can be seen in Fig. 3. In Fig. 3(a), the design is composed of 128 microphone units, which are grouped into eight circular subarrays with each subarray having 16 microphones. It can be seen from Figs. 1(d)-1(f) that the zeros of Bessel functions are eliminated within $0-8$kHz. The radii of neighboring subarrays form a generalized arithmetic sequence. It is also possible to distribute the microphones in other ways such as four subarrays with 32 microphones each or 64 subarrays with two microphones each. Figure 3(b) shows another possible distribution of microphone units, which also consists of eight circular subarrays, but three pairs of subarrays have the same radii with different rotation angles. The angle of rotation of the subarrays may be arbitrary, such as in Figs. 3(c) and 3(d). However, all the microphone units are placed in an equiangular manner.

The strength of the proposed design is the capability of performing error-robust broadband sound field recording with omnidirectional microphones and no redundant units located in the same direction. The multi-subarray design allows higher angular sampling density without using very small microphone units.

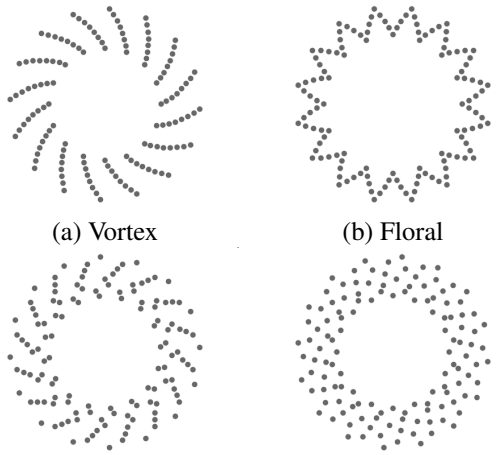

(a) Vortex (b) Floral

(c) Random 1 (d) Random 2

Fig. 3: Some examples of proposed designs ($Q = 128$).

4 Spatial Resolution Control

According to (4), the transform matrix B_k is frequency-dependent due to its mode function $b_n(kr)$. At low frequencies, the value of the mode function approaches zero when the order n increases; this phenomenon can be observed in Fig. 1. This indicates that the transform matrix is overdetermined. Inverting an overdetermined matrix should only involve its prominent components, otherwise the inversion is ill-conditioned. Spatial resolution control trims the rows of the transform matrix, reducing its spatial resolution in exchange for obtaining a well-conditioned pseudoinverse, $B_k^{\dagger}$. This can be interpreted as a variant of TSVD (truncated singular value decomposition) regularization. The main difference is that TSVD operates in a matrix's left-singular domain, while spatial resolution control operates in the spherical or cylindrical mode domain. It has also been recommended in multiple papers [4] [11] that choosing an appropriate spatial resolution for different frequencies can result in better robustness.

In the cases of a Bessel or spherical Bessel function, these functions quickly approach zero after their order n surpasses a threshold, $n_0(kr)$. The selection of the spatial resolution is the same as determining the threshold value $n_0(kr)$. If $n_0(kr) < N_{arr} = \lfloor (Q-1)/2 \rfloor$, then the spherical or cylindrical harmonic terms between $n_0(kr)$ and N_{arr} do not significantly contribute to the sound field reconstruction. Omitting these negligible terms in the reconstruction stage improves the condition of the transform matrices with the loss of only a marginal amount of information. Therefore, we can now construct the spatial-resolution-controlled transformation matrix $B_k^{n_0}$, which contains only the first $n_0(k \times \max(r))$ rows of the original B_k (introduced in (4)). The function $n_0(kr)$ can be defined in many ways. One straightforward definition is $n_0(kr) = \rho kr$, where ρ is 1 [4] or 1.1 [11]. Another possible definition, which determines n_0 according to the p-norm of $b_n(kr)$, is proposed here:

$$n_0(kr) = \inf_n \frac{\sum_0^N \|b_n(kr)\|_p}{\sum_0^\infty \|b_n(kr)\|_p} > \rho,\ |\rho| < 1,\ 1 \le p \le 2. \tag{7}$$

The threshold value ρ in (7) is preferably close to 1 and p is 2. All the figures in this paper related to spatial control use the definition of n_0 in (7). The effect of spatial resolution control will be discussed in section 6.

5 Parameter Optimization

As described in section 3, it is difficult to utilize a gradient-based algorithm to minimize the condition number of matrix in general. Therefore, the differential evolution algorithm is used [18]. Although differential evolution is not guaranteed to deliver an optimal solution, it has been widely used for nonsmooth and constrained optimization [19].

The optimal values of the actual parameters of the proposed design are determined on the basis of these constraints:

Number of microphone units Q
: This determines the possible numbers of subarrays. For example, if 24 microphones are used, then it is possible to have 1, 2, 3, 4, 6, 12, or 24 subarrays.

Operating frequency range f_{min}, f_{max}
: The conditioning of transform matrices with respect to this frequency range will be examined in the optimization process.

Diameter of microphone unit D_m
: This defines the minimal magnitude of the common difference in the generalized arithmetic sequence for subarray radii. The minimal difference between the radii of neighboring subarrays can be represented as

$$|r_i - r_j| \leq r_j\Big(\cos\Big(\frac{2\pi}{Q}\Big) - 1 + \sqrt{\Big(\frac{D_m}{r_j}\Big)^2 - \sin^2\Big(\frac{2\pi}{Q}\Big)}\Big), \quad i \neq j. \quad (8)$$

Upper bound of condition number κ_{max}
: This is the highest acceptable condition number within the operating frequency range. Empirically, if the condition number is larger than 100, the matrix inverse will become ill-conditioned, and thus unstable. However, in some cases, if multicollinearity is undesirable, κ_{max} should be set to around 30 [20].

With the above constraints, the next step is to find the optimal values of the number of subarrays S, the radius of each subarray $r = [r_0, r_1, \ldots, r_{S-1}]$, and the angle of rotation of each subarray $\phi = [\phi_0, \phi_1, \ldots, \phi_{S-1}]$. With these parameters, the actual geometry can be derived.

The optimal parameter set $P^Q_{opt} = \{S, r, \phi\}$ is the one minimizing the average condition number of the transform matrices B_k within $[f_{min}, f_{max}]$ subject to the constraints of D_m and κ_{max}.

A prototype microphone array based on the layout depicted in Fig. 3(a) (Vortex) was built. It is composed of 128 omnidirectional electret condenser microphones, each with a diameter of 2.1cm. The array aims to operate within 0–8kHz frequency range, which is the crucial band for sound localization in the human auditory system [21]. The upper limit of the matrix condition number is set to 30. In accordance with these conditions, an approximately optimal parameter set is found.

An actual sound field recording experiment using the prototype array was conducted in an audio room of size 5.4m × 6.7m × 3m. The measured sound pressure and reconstructed sound field are respectively shown in Figs. 4 and 5. The background noise is approximately $-30dB$ and the room is reverberant. The spatial resolution control is applied in the reconstruction stage and the threshold n_0 is determined by (7). Since r in (7) is the radius of the largest subarray, the area with the approximately correct reconstruction should roughly lies within the outer circumference of the array.

The array in Fig. 3(b) (Floral) is another approximately optimal solution if subarrays can have the same radius. In addition to Vortex and Floral, two other designs are shown, referred to as Random 1 (Fig. 3(c)) and Random 2 (Fig. 3(d)). These two designs have the same parameters as Vortex but the rotation angles of their subarrays are randomized. These designs do not result from any optimization but are merely examples to show how the parameters may affect the condition numbers of the transform matrices, which will be discussed in the next section.

$f = 1041Hz$ $f = 3305Hz$

Fig. 4: Measured pressure values. A speaker is located 1m away in front of the array (i.e. speaking from the top of the figure). The side length of the grid is 0.5m.

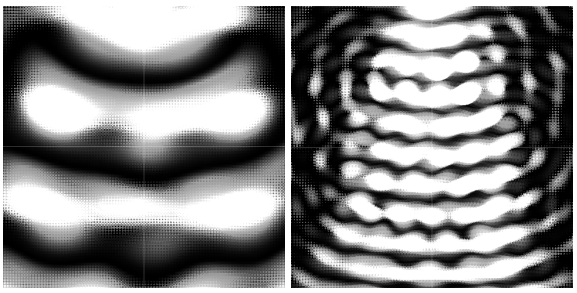

$f = 1041Hz$ $f = 3305Hz$

Fig. 5: Sound field reconstructed from the measured pressure values.

6 Error Robustness Analysis

The error robustness of an array geometry is indicated by the average of condition numbers of its transform matrices. The condition numbers can be decreased by reducing the spatial resolution, in other words, reducing the number of modes contained in the transform matrices. In this section, we will first examine the error robustness of several array geometries, then investigate

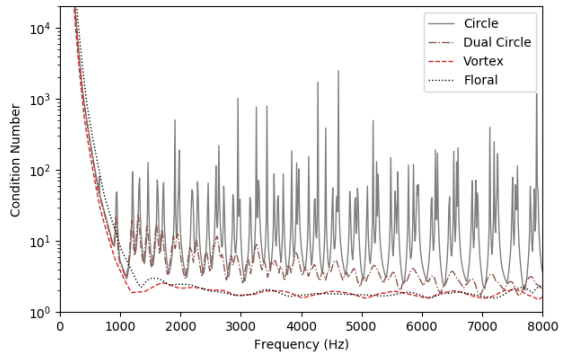

(a) $N = 6$

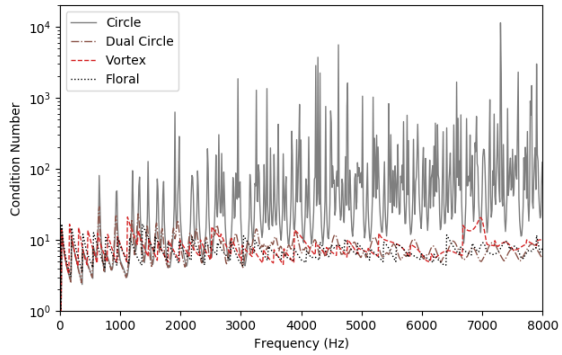

(b) $N = n_0(kr)$

Fig. 6: Condition number between 0 and 8kHz for different microphone arrays. (a) Condition number curves when the spatial resolution is fixed at $N = 6$, (b) condition number curves when the spatial resolution is frequency-dependent, where the spatial resolution is determined by $N = n_0(kr)$ as in (7).

how the number of usable modes changes when the upper limit of the condition number decreases.

6.1 Effectiveness of Spatial Resolution Control

The effect of spatial resolution control is crucial in low-frequency bands. Since in low-frequency bands, the sound field complexity is limited [3], removing excessive dimensions in overdetermined systems improves the system condition. The condition number curves of various arrays before and after spatial resolution control are shown in Fig. 6. As can be seen from the figure, if no spatial resolution control is applied, the condition of transform matrices at low-frequency bands is extremely poor (Fig. 6(a)). Fig. 6(b) shows that after spatial resolution control is applied, the condition number for most of the frequency bands is controlled within 30 for all arrays except the circular array. The ill-condition of the circular array is caused by the Bessel zero problem, which is an inherent property and cannot be solved by spatial resolution control. Although the ill-condition of the circular array may be improved by ordinary regularization, the information of absent modes cannot be recovered, therefore the reconstructed sound field will lack some modes at these frequencies.

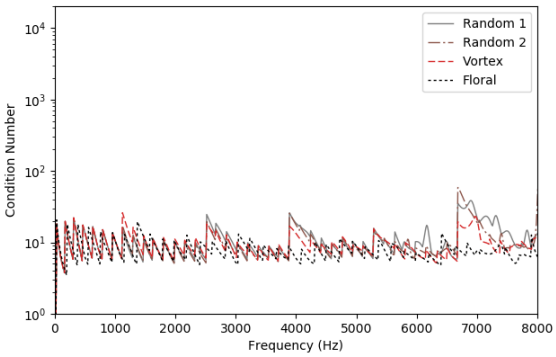

Fig. 7: Condition number plot within 0–8kHz for the designs in Fig. 3 in the case of controlled spatial resolution.

6.2 Effect of Angular Rotation

According to (4), in contrast to the conventional circular array, the mode function of the proposed design is coupled with spherical/cylindrical harmonic coefficients within the transform matrices. According to our preliminary observation, the local optimum evaluated by metaheuristic algorithms appears to favor those with lower discontinuity in the angular domain.

As shown in Fig. 7, the example from Fig. 3(b) (Floral) has the lowest discontinuity and the best average transform matrix condition among the four arrays in Fig. 3. On the other hand, the microphone placement of Fig. 3(a) (Vortex) has a larger radial difference every eight units, therefore the condition is slightly worse. The performance of random placements is even worse, probably due to the higher discontinuity. Despite the experimental observation, the effect of this coupling requires further investigation.

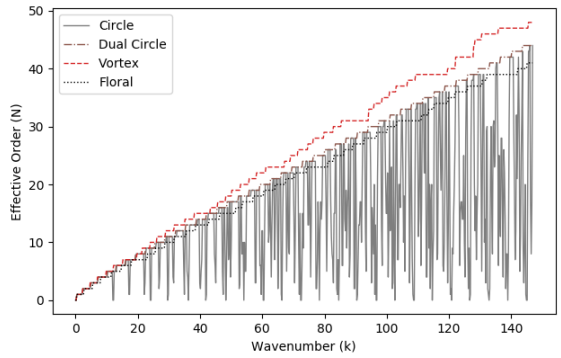

Fig. 8: Effective cylindrical harmonic order of various 2D arrays with spatial resolution control applied ($\kappa_{max} = 30$).

6.3 Effective Order in Mode Domain

To compare the performance between the proposed geometries and conventional circular arrays, we require a feasible performance measure. In this section, we use the effective order of a matrix to act as the performance measure.

We know that if the upper limit of the condition number κ_{max} is fixed, then the rank of the transform matrix pseudoinverse $B_k^{\dagger}$ indicates the amount of recoverable information contained in the matrix. In cylindrical/spherical domain processing, the rank of the transform matrix is related to order. A higher order means a larger reconstructible area, more modes are required at a higher frequency to achieve the same reconstructible area. However, if some of the modes are missing in the regularized pseudoinverse, even if the matrix rank is high, the reconstructed sound field is still incomplete. In this case, the effective order of this matrix should be regarded as the lowest order of the missing modes minus one. Otherwise, the effective order is equal to the maximum order among the modes.

The effective order of various 2D arrays within the $0-8$kHz frequency range is plotted in Fig. 8. In the figure, the proposed geometries (Vortex, Floral) clearly have higher effective order than the circular array on average within this frequency range. The circular array is strongly affected by the Bessel zero problem and therefore has a low effective rank in several frequency bins. A dual circle solves the problem but requires twice the number of microphone units. Note that the effective orders of the proposed arrays rapidly decrease outside of the range of frequency of interest, while the effective orders of circular and dual circular arrays continually repeat their own behavior in Fig. 8.

Although the Vortex geometry slightly outperforms Floral geometry, the Floral geometry seems to be more resilient when the upper limit of the condition number becomes tight, as shown in Fig. 9. This indicates that if the recording environment is noisy or the SNR of the microphones is low, the Floral geometry may be a more suitable choice.

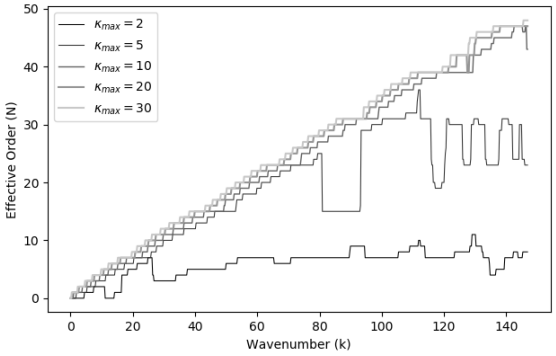

(a) Vortex, $k = 2\pi f/c_s$, f: $0-8$kHz

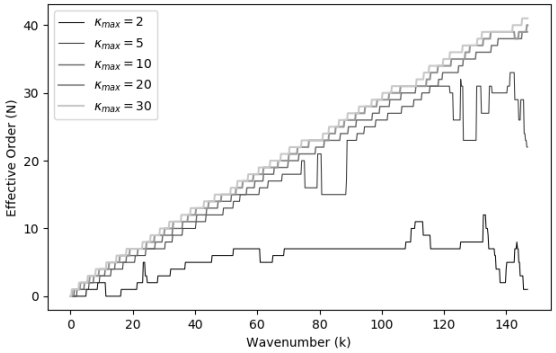

(b) Floral, $k = 2\pi f/c_s$, f: $0-8$kHz

Fig. 9: Applicable cylindrical harmonic orders of proposed arrays within frequency range $0-8$kHz under different κ_{max} constraints.

7 Conclusion

In this article, in accordance with the relationship between the Bessel zero problem and error robustness [9], we proposed a parametric geometry design of 2D arrays with strong error robustness that can achieve better sound field recording than the conventional circular or

dual circular array in terms of the reconstructible area over a broad frequency range.

The design constructs an array with multiple circular subarrays in such a way that all the microphones are equally distributed in the angular domain with the radii of the subarrays forming a generalized arithmetic sequence. The parameters of such an array are dependent on several predetermined constraints, and the approximate optimal parameters can be found by using metaheuristic algorithms.

An actual prototype device was built and a preliminary sound field recording experiment was conducted. The performance in a practical environment will be evaluated in detail in future.

Since the design introduces coupling between the radial and angular components, the effect of such coupling should be investigated in future. It would also be valuable to develop source localization and tracking algorithms based on the proposed geometries.

References

[1] Ahrens, J., *Analytic Methods of Sound Field Synthesis*, Springer Berlin Heidelberg, 2012.

[2] Candès, E. and Romberg, J., "Sparsity and Incoherence in Compressive Sampling," *Inverse Problems*, 23(3), pp. 969–985, 2007, doi:10.1088/0266-5611/23/3/008.

[3] Kennedy, R. A., Sadeghi, P., Abhayapala, T. D., and Jones, H. M., "Intrinsic Limits of Dimensionality and Richness in Random Multipath Fields," *IEEE Transactions on Signal Processing*, 55(6), pp. 2542–2556, 2007, doi:10.1109/tsp.2007.893738.

[4] Rafaely, B., *Fundamentals of Spherical Array Processing*, Springer Berlin Heidelberg, 2015.

[5] Williams, E. G., *Fourier Acoustics: Sound Radiation and Nearfield Acoustical Holography*, Academic Press Inc., 1999, ISBN 0127539603.

[6] Balmages, I. and Rafaely, B., "Open-Sphere Designs for Spherical Microphone Arrays," *IEEE Transactions on Audio, Speech and Language Processing*, 15(2), pp. 727–732, 2007, doi:10.1109/tasl.2006.881671.

[7] Huang, G., Benesty, J., and Chen, J., "Design of Robust Concentric Circular Differential Microphone Arrays," *The Journal of the Acoustical Society of America*, 141(5), pp. 3236–3249, 2017, doi:10.1121/1.4983122.

[8] Jarrett, D. P., Habets, E. A. P., Thomas, M. R. P., and Naylor, P. A., "Rigid Sphere Room Impulse Response Simulation: Algorithm and Applications," *The Journal of the Acoustical Society of America*, 132(3), pp. 1462–1472, 2012, doi:10.1121/1.4740497.

[9] Rafaely, B., "The Spherical-Shell Microphone Array," *IEEE Transactions on Audio, Speech, and Language Processing*, 16(4), pp. 740–747, 2008, ISSN 1558-7916, doi:10.1109/TASL.2008.920059.

[10] Proakis, J. G. and Manolakis, D. K., *Digital Signal Processing (4th Edition)*, Prentice Hall, Inc., 2006, ISBN 0131873741.

[11] Jarrett, D. P., Habets, E. A. P., and Naylor, P. A., *Theory and Applications of Spherical Microphone Array Processing*, Springer International Publishing, 2016.

[12] Trefethen, L. N. and Bau, D., *Numerical Linear Algebra*, SIAM, 1997, doi:10.1137/1.9780898719574.

[13] Betlehem, T. and Abhayapala, T. D., "Theory and Design of Sound Field Reproduction in Reverberant Rooms," *The Journal of the Acoustical Society of America*, 117(4), pp. 2100–2111, 2005, doi:10.1121/1.1863032.

[14] Winter, F., Ahrens, J., and Spors, S., "On Analytic Methods for 2.5-D Local Sound Field Synthesis Using Circular Distributions of Secondary Sources," *IEEE/ACM Transactions on Audio, Speech, and Language Processing*, 24(5), pp. 914–926, 2016, ISSN 2329-9290, doi:10.1109/TASLP.2016.2531902.

[15] Maréchal, P. and Ye, J. J., "Optimizing Condition Numbers," *SIAM Journal on Optimization*, 20(2), pp. 935–947, 2009, doi:10.1137/080740544.

[16] Underbrink, J., "Circularly Symmetric, Zero Redundancy, Planar Array Having Broad Frequency Range Applications," 2001, US Patent 6,205,224.

[17] Prime, Z. and Doolan, C., "A Comparison of Popular Beamforming Arrays," in *Proceedings of Acoustics 2013, Annual Conference of the Australian Acoustical Society*, 2013.

[18] Storn, R. and Price, K., "Differential Evolution – A Simple and Efficient Heuristic for Global Optimization over Continuous Spaces," *Journal of Global Optimization*, 11, pp. 341–359, 1997, ISSN 1573-2916, doi:https://doi.org/10.1023/A:1008202821328.

[19] Sayah, S. and Zehar, K., "Modified Differential Evolution Algorithm for Optimal Power Flow with Non-smooth Cost Functions," *Energy Conversion and Management*, 49(11), pp. 3036–3042, 2008, doi:10.1016/j.enconman.2008.06.014.

[20] Belsley, D. A., Kuh, E., and Welsch, R. E., *Regression Diagnostics*, John Wiley & Sons, Inc., 1980, doi:10.1002/0471725153.

[21] Morikawa, D. and Hirahara, T., "Signal Bandwidth Necessary for Horizontal Sound Localization," in *Proceedings of 20th International Congress on Acoustics, ICA 2010*, 2010.